ARTIFICIAL NEURAL NETWORK FOR TEXTURE CLASSIFICATION USING SEVERAL FEATURES: A COMPARATIVE STUDY

Mohammed W. Ashour, Khaled M. Mahar, and Mahmoud F. Hussin

College of Engineering & Technology, Arab Academy for Science & Technology and Maritime Transport, Alexandria, Egypt
eng.m.ashour@gmail.com, khmahar@aast.edu, mfarouk@pami.uwaterloo.ca

ABSTRACT

*Texture analysis plays an essential and a major rule in image classification and segmentation in a wide range of applications such as medical imaging, remote sensing and industrial inspection. In this paper, we review the well known approaches of texture feature extraction and perform a comparative study between them. These approaches are namely gray level histogram, edge detection, and co-occurrence matrices, besides Gabor and Biorthogonal wavelet transformations. The feed forward artificial neural network (**ANN**) with **b**ack- **p**ropagation **a**lgorithm (**BPA**) is used as a supervised classifier. Experiments are conducted on two different datasets taken from multi-class engineering surfaces produced by six machining processes and from **Brodatz (1966)** textures album respectively. The classification accuracy is tested for both datasets, while the quality of estimation is tested for surface roughness parameters of the machined surfaces dataset only based on the roughness parameters evaluated from a contact measurement test.*

Keywords**:** *Feature extraction, Supervised neural network, Texture Classification.*

1. INTRODUCTION

Texture analysis is defined as the classification or segmentation of textural features with respect to the shape of a small element, density and direction of regularity [1]. A number of texture feature extraction approaches have been proposed in the literature such as neighborhood relationships, Fourier transform, numerically calculated parameters, wavelet transform, and multi-resolution analysis. Haralick et al. [2] used the neighborhood relationships for intensity matrix to extract features from the texture. Also, Wei Min Shi et al. [3] proposed a pattern recognition theory to perform surface roughness classification by comparison with known surfaces. While, Sin-Wang-Sonei et al. [4] attempted to detect and classify surface defects, in textured materials using wavelet packets. Shmuel Peleg, [5] presented a method for texture classification based on the change in the properties of the images with the change in its resolution. Yun Zhang1- et al. [6] focused on the development of a wavelet-integrated technique for star amplitude radar images (***SAR***) and multi-spectral images fusion. For roughness estimation, Kuang-Chyi et al. [7] discussed the estimation of surface roughness of workpieces in turning operations. Luk et al. [8] utilized statistical parameters, derived from the gray level intensity histogram such as the range and mean value of the distribution and correlated them with the roughness value (R_a) determined from the stylus method.

In this paper, we use the gray level histogram, edge detection, co-occurrence matrices, Biorthogonal wavelet transform and Gabor wavelet transform as feature extraction techniques. An input vector of significant features is taken for some tested samples to analyze and classify its texture and to estimate R_a of the machined textures also without contact by using the ***ANN*** classifier. A supervised classifier based on a feed forward back- propagation neural network is proposed, it uses an adaptive learning rate with momentum term algorithm.

The recently research in texture classification is usually depends on supervised classifiers such as supervised ***ANN*** and Support Vector Machines (***SVM***) or unsupervised classifiers such as Self Organizing Maps (***SOM***). For example, Roberto Marmo et al. [9] used the supervised ***ANN*** to classify carbonate rock textures based on the digitized images of thin section rocks. S. Arivazhagan et al. [10] has found texture features by calculating the mean and variance of the Gabor filtered image, and achieved rotation normalization by the circular shift of the feature elements, then texture similarity measurement of the query image and the target image in the database was computed by minimum distance criterion. Chih-Ming Chen et al. [11] used the texture features derived from Gabor and other four wavelet transforms for classification and clustering based on ***SVM*** and ***SOM***, with a comparison between both techniques to show that these appropriate classifiers perform reasonably well. The encouraging and experimental results show that the suggested methodology can identify and classify the type of the machining process used to produce the work-pieces and also can classify the Brodatz patterns by a supervised ***ANN***.

The reminder of this paper is organized as follows. The proposed algorithm can be divided entirely into two main parts: the texture analysis and texture classification. In section 2 the methodology applied in our experiment is discussed with a brief overview on the proposed techniques in texture analysis and features extraction, also it contains the detailed description of the texture classification part with the supervised artificial neural network classifier and its phases. Section 3 contains the discussions and the analysis of

the proposed algorithm experimental results. Finally section 4 concludes the paper.

2. THE METHODOLOGY

The aim of this paper is to provide a wide comparison between some different schemes in texture feature extraction, as illustrated in Figure 1 the proposed algorithm is divided into three stages, in the first one features extraction methods which are histogram, edge detection, co-occurrence matrices, Biorthogonal wavelet transform and Gabor wavelet transform are applied to our texture image, then secondly the input feature vector is selected for each image to be classified in the third stage by the ***ANN*** classifier, after that the R_a parameter is estimated for the machined dataset surfaces and compared with the measured R_a. The following sections are describing these stages in details.

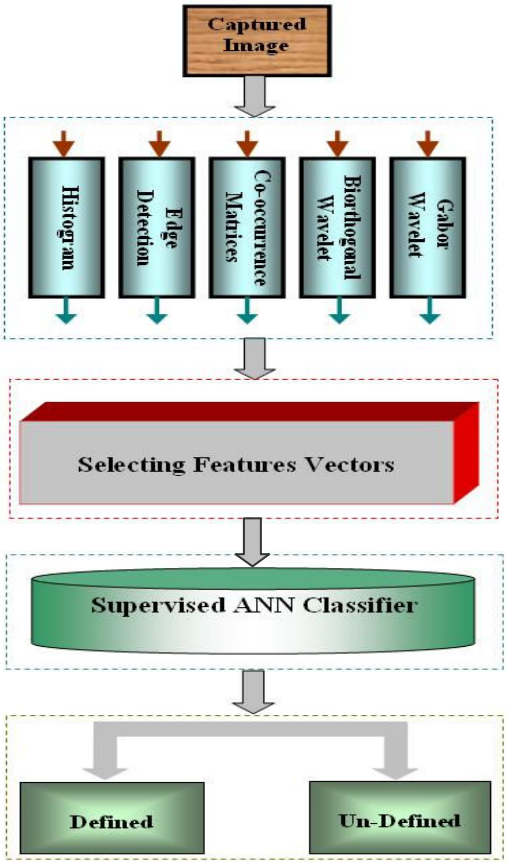

Figure 1: Experimental Setup.

2.1 FEATURE EXTRACTION METHODS AND SYSTEM SETUP

2.1.1 GRAY LEVEL HISTOGRAM

The histogram is the number of occurrences of each gray-level intensity in an image [16]. The histogram of each image gives a vector of length **256**. The output of histogram algorithm for all specimens gives 36 vectors each with **256** values; these vectors are divided into six matrices according to class type, each of size (256*6) and then are used as an input to the ***ANN***.

2.1.2 EDGE DETECTION METHOD

The edge is characterized by an abrupt change in intensity indicating the boundary between two regions in an image, which have different gray-level values, and is often referred to as a discontinuity. Edge detection is usually based on the calculation of intensity gradients across the image. Figure 2 shows the detected edges for an image. The occurrence of a high local intensity gradient, indicating a sudden intensity transition, and is evidence for the existence of an edge discontinuity [17]. The edges are extracted from the machined surface images at 0 and 90 degree of rotation horizontally and vertically to have new images with edges detected. Then, the mean and variance of each image are calculated and stored respectively in a vector at column shape with length equals the number of columns (1280*2) elements, that's applied for all images of specimens giving 36 columns, each has 2560 elements. These vectors are divided into six matrices according to class type, each of size (2560*6) and are used as an input to the ***ANN***.

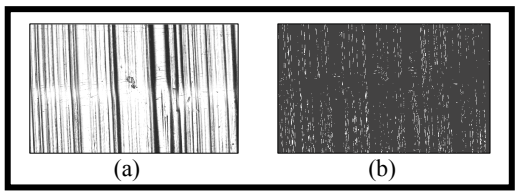

Figure 2: (a) Original image, (b) Detected edges.

2.1.3 GRAY LEVEL CO-OCCURRENCE MATRICES

The co-occurrence matrix is generally referred to as gray-level co-occurrence matrix whose entries are transitions between all pairs of two gray levels [18]. The gray-level transitions are calculated based on two parameters, displacement and angular rotation, giving four gray-level co-occurrence matrices at ***0, 45, 90,135*** degrees orientation as shown in Figure 3.

In Figure 3 cells 1&5 are 0^0, cells 2 & 6 are 135^0, cells 3&7 are 90^0, and cells 4 & 8 are 45^0 nearest neighbors. For an image having a spatial resolution $N_x * N_y$ and gray scale level ***256***, the angular relationship between pairs at distance ***d=1*** between pixels is as follows:

At 0^0 orientations (horizontal) the co-occurrence matrix contains $2N_y (N_x-1)$ nearest horizontal neighbor pairs.

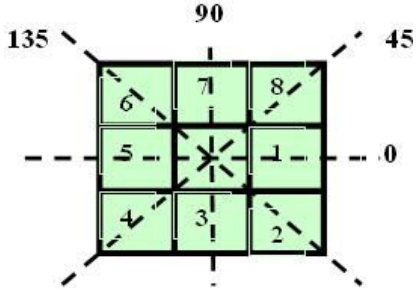

Figure 3: Neighbors relationship.

At 45^0 orientation (right diagonal) the co-occurrence matrix contains $2(N_y-1)(N_x-1)$ nearest right diagonal neighbor pairs. By symmetry there will be $2N_y(N_x-1)$ nearest vertical neighbor pairs and $2(N_y-1)(N_x-1)$ nearest left diagonal neighbor pairs [18].

In this method the mean and variance of Neighbors relationship at 0^0 and 180^0 orientations are collected together at one vector of $(512+512)$ for each specimen image giving 36 columns, each has 1024 elements to be used as an input to the *ANN* supervised classifier.

2.1.4 WAVELET TRANSFORMATIONS

The WT of a continuous function $s(t)$ is given by:

$$W_{a,\tau} = \frac{1}{|a|^{\frac{1}{2}}} \int_{-\infty}^{\infty} \psi\left(\frac{t-\tau}{a}\right) s(t)\, dt \qquad (1)$$

Where, a and τ are the dilation and translation parameters. $W_{a,\tau}$, is the wavelet transform of $s(t)$. In the most common formulation; $a = 2^{-j}$.
The translation is discredited with respect to each scale by using $\tau = k2^{-j}T$.
In this case, the wavelet basis functions are obtained by

$$\psi_{j,k}(t) = 2^{j/2}\psi(2^j t - kT) \qquad (2)$$

The two parameters expansion of a signal is termed as particular wavelet basis functions (or wavelets) $\psi(t)$,and scaling function $\varphi(t)$. The wavelet decomposition of a signal is obtained by convolving the signal with a family of real orthonormal basis functions $\psi_{jk}(t)$ [19]; where k represents translation of the wavelet function of time, while integer j, however, is an indication of the wavelet frequency and generally referred to as scale (higher scale corresponds to finer localization and vice versa). The two wavelet parameters scaling $\phi(t)$ and wavelet basis $\psi(t)$ are utilized as expressed by [19]

$$s(t) = A_k\phi_{j_0,k}(t) + \sum_{j=j_0}^{\infty} D_{j,k}\psi_{j,k}(t) \qquad (3)$$

where:

k: an integer representing the transformation of the wavelet function and indication of time or space in wavelet transform.

j: an indication of the wavelet frequency or spectrum.

A_k: approximation coefficient.

$D_{j,k}$: represents the details of the signal at different scales.

ψ: is used to define the details, and

ϕ: . is used to define the approximations.

Wavelet can be divided into different classes and in many different ways. The most commonly used classes can be categorized into two classes Orthogonal and Biorthogonal wavelets.

2.1.4.1 ORTHOGONAL WAVELET

In this system the analysis (the decomposition) and the synthesis (the reconstruction) filters are not symmetric, and the order of filters is always an even number. Orthogonal wavelets are very successful in numerical analysis like solving partial differential equations, speech coding and other similar applications, where symmetry is not a major requirement.

2.1.4.2 BIORTHOGONAL WAVELET

In this system the decomposition and reconstruction filters can be forced to be symmetric. For $\psi_{7,11}$, $\Phi_{7,11}$ the 1^{st} number represents the order of a low pass filter (LPF) for decomposition, while the 2^{nd} number represents the order of reconstructed LPF [9].
In image processing applications, Bi-orthogonal wavelets, which are symmetric, are more desirable. Symmetric wavelets allow extension at the image boundaries and prevent image contents from shifting between sub-bands.

The two-dimensional wavelet transform (*2-DWT*) for image application leads to a decomposition of approximation coefficients at level j in four components as shown in figure 4, the approximation at level $j+1$, and the details in three orientations (horizontal, vertical, and diagonal).

In this paper, since our aim is to classify, identify and estimate the surface roughness parameter for the engineering surfaces dataset, we will have to extract the most high frequency components from these images to get a better performance from our technique, so we apply two dimensional Biorthogonal wavelet transform to the tested images, then we extract from the transform coefficients the three details (horizontal, vertical, and diagonal) with orientations 0^0, 90^0, 45^0 respectively.

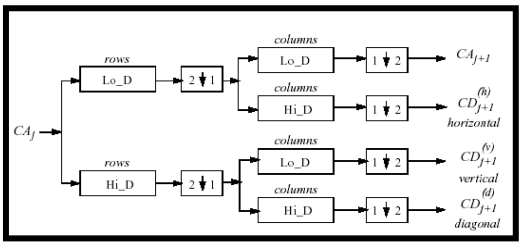

Figure 4: Two Dimensions wavelet transformation.

We have performed several tests on different types of features, the final set is composed of the following:
1- Sum: is the sum of pixels values in a detail component [8].
2- Maximum: is the largest element along different dimensions of an array.
3- Minimum: is the smallest element along different dimensions of an array.
4- Mean: is the mean value of the elements along different dimensions of an array.
5- Standard deviation (std): for a 2-D matrix is a row vector containing the standard deviation of the elements in each column and can be expressed as.

$$s=\left(\frac{1}{n}\sum_{i=1}^{n}(x_i-\bar{x})^2\right)^{\frac{1}{2}}, \textit{ where } \bar{x}=\frac{1}{n}\sum_{i=1}^{n}x_i \quad (4)$$

6- Median: is the median values of the elements along different dimensions of an array.
7- Range: is the minimum and maximum values vector of elements along different dimensions.
8- Rz: is known as the ISO 10 point height parameter in ISO 4287/1-1948, is measured on the roughness profile only and is numerically the average height difference between the five highest peaks and the five lowest valleys within the sampling length [14].
9- R3y: the deviation from the third highest peak to the third lowest valley in each sample length is found, R3y is then the largest of these values [14].
10- R3z: is the vertical mean from the third highest peak to the third lowest valley in a sample length over the assessment length [14].
11- Energy: is the percentage of energy corresponding to the approximation, and it is extracted from the wavelet decomposition coefficients.

The previous 11 features are extracted from the three details produced by transforming one image, and then collected to gather, in order to have finally a single vector of length 33 elements representing each image. These output vectors are divided into six matrices according to class type, each matrix of size (33*6) and then are used as an input to the ***ANN***.

2.1.5 GABOR WAVELET TRANSFORM

A Gabor function is the product of a Gaussian function and a complex sinusoid, a two dimensional Gabor function g(x,y) and its Fourier transform G(u,v) can be written as [10]

$$g(x,y)=\frac{1}{2\pi\sigma_x\sigma_y}\exp\left(\frac{-1}{2}\left(\frac{x^2}{\sigma_\sigma^2}+\frac{y^2}{\sigma_y^2}\right)+2\pi jWx\right) \quad (5)$$

$$G(u,v)=\exp\left(\frac{-1}{2}\left(\frac{(u-W)^2}{\sigma_u^2}+\frac{v^2}{\sigma_v^2}\right)\right) \quad (6)$$

Where,

$$\sigma_u=\frac{1}{2\pi\sigma_x},\quad \sigma_v=\frac{1}{2\pi\sigma_y}$$

Gabor functions form a complete but non-orthogonal basis set. Expanding a signal using this basis provides a localized frequency description.

A class of self-similar functions referred to as *Gabor wavelets*, is now considered. Let *g(x,y)* be the mother Gabor wavelet, then this self-similar filter dictionary can be obtained by appropriate dilations and rotations of g(x,y) through the generating function :

$$g_{mn}(x,y)=aG(x',y') \quad (7)$$

$$a>1$$

m,n Integers

and $x'=a^{-m}(xCos\theta+ySin\theta)$ (8)

$$x'=a^{-m}(-xSin\theta+yCos\theta) \quad (9)$$

Where

$$\theta=\frac{n\pi}{k}$$

and k is the total number of orientations. The scale factor is a^{-m} meant to ensure that the energy is independent of m.

Feature extraction using Gabor functions is motivated by the fact that, these filters can be considered as orientation and scale tunable detectors. Here, in this method the output is obtained by applying Gabor filter on each texture image for 12 different orientations in steps of 30^0, and a constant values for variances along x and y-axes (S=0.05, F=0.025) respectively, and phase (P= 0), after that the mean and standard deviation of all transformed coefficients are found, these features are collected together in one single vector of length (12*2=24) elements to represent each image and then used as an input to the ***ANN***.

2.2 ARTIFICIAL NEURAL NETWORK CLASSIFIER

The used supervised classifier is based on a feed forward back- propagation neural network, which uses an adaptive learning rate with momentum term algorithm; this classifier is constructed and trained with the following configuration and parameters:

- Three layer architecture, i.e. one hidden layer.
- Number of nodes in the input layer equal to the length of input vector.
- Output layer is an identity matrix with diagonal length equal to the number of input at each batch network.
- Type of activation function between input and hidden layers is tan-sigmoid but the function between hidden and output layer is pure line.
- The maximum epochs for training = 10000.
- The error goal =0.0001.
- The display frequency =50.

In training mode the same ***ANN*** architectures is used and trained for two different datasets separately. In order to be able to test unlimited number of samples we chose to train each 6 samples together in one independent ***ANN***.

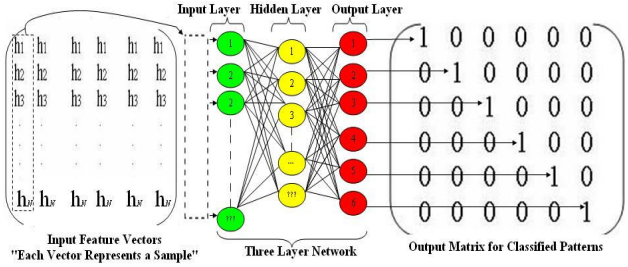

Figure 5: Three layers feed-forward neural network showing its inputs and outputs.

Then at the recalling mode we call all the trained samples for each testing. Figure 5 illustrates the used neural network with its inputs and outputs. When classification is done using any of the proposed textural analysis methods, the classifier receives six input matrices from each method for the machined surfaces dataset, and eight matrices from each method when classifying Brodatz textures. Each matrix is trained using one different network by passing the matrix columns one by one to the input layer of the network, and then weights and biases are saved for recalling mode. Once the training has been performed, a test mode is applied to ensure that the network will give the same response and produce the same desired output when the same input is applied at any time (i.e. classify the specimens).

3. EXPERIMENTAL WORK AND RESULTS

3.1 FIRST DATASET

The first used dataset consists of 36 samples of multi-class engineering surfaces produced by six machining processes namely, turning, grinding, Horizontal-milling, vertical-milling, lapping and shaping [11]. Turning is the operation of producing surfaces of rotation using a single point cutting tool but in grinding the material is removed by means of a rotating abrasive wheel to obtain better surface finish, and Milling is the process of removing material from the surface of the work piece by feeding the work-piece past a rotating multipoint cutter, while Lapping is the final abrasive finishing operation that produces extreme dimensional accuracy, corrects minor imperfections of shape, refines surface finish, and produces close fit between mating surfaces. Shaping can be defined as the oldest single point machining process since it uses a straight-line cutting motion to generate a flat surface [14]. Some preprocessing work is needed to be done before getting the tested image ready. Firstly, we prepare our 36 real specimens using the specified six machining processes then the roughness $\boldsymbol{R_a}$ of its surfaces is measured using a precise stylus instrument form Talysurf series-2 instrument and store this data as a reference on our PC to be compared with the estimated ones when applying our technique later, after that we acquire images for the textures of size 1024 × 1280 using a precision camera to be our first dataset.

3.1.1 ROUGHNESS MEASUREMENTS

Roughness is one of the main components in engineering surfaces texture; it can be expressed using the following sets of parameters:

- Amplitude parameters: measure the vertical characteristics of the surface deviations.
- Spacing parameters: measure the horizontal characteristics of the surface deviations.
- Hybrid parameters: which are combinations of both horizontal and vertical deviations [8].

These parameters are measured along a profile produced by a precise instrument traveling across the surface. The profile is divided into sample lengths, which are long enough to include a statistically reliable amount of data, yet short enough to exclude undesired data from the measurement.

The amplitude parameters include: $\boldsymbol{R_a}$ or the average roughness value (the universally recognized and most used international measure of roughness) and it is calculated as follows:

$$R_a = 1/L_r \int_0^{L_r} |Z(x)| \quad dx \tag{10}$$

Where:

Lr is the length in the direction of x axis used for assessing the profile under evaluation, and Z(x) is the amplitude along the line profile [15].

3.1.2 IMAGE ACQUISSITION

This stage describes the process of converting the picture into its numerical representation, which is suitable for further image processing steps. Intensity images with 256 linear gray tones (zero corresponds to black color and 255 to white), were captured for test specimen surfaces. The surfaces were viewed under an optical microscope equipped with a digital camera. Captured images were also stored in a PC for further analysis.

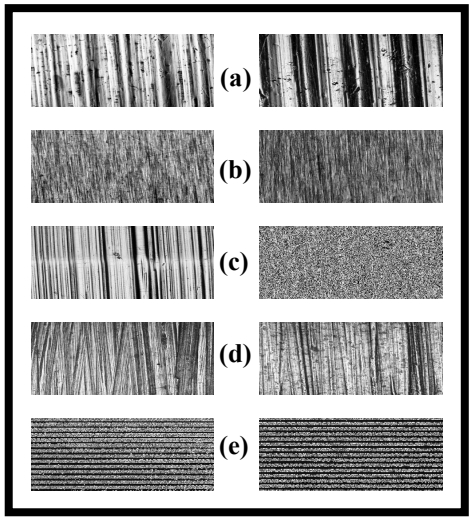

Figure 6: Different machined processes samples, (a), (b), (c), (d) and (e) are turning, grinding, milling, lapping and shaping respectively.

3.1.3 RESULTS

The experimental results of the different five textural features extraction techniques using the machined textures dataset were as follows:

- The Histogram method gives number of input neurons (256) to the ***ANN*** with number of hidden neurons equal to (200), which implies an average simplicity for the ***ANN*** architecture, and it has (16/36) samples are having minimum error in Ra estimation, regarding its accuracy (97.22%) for each sample.
- The edge detection method gives highest number of input neurons (2560) in the ***ANN*** and it gives number of hidden neurons equal to (200), which implies the most complex ***ANN*** architecture, and it

has the lowest number (12/36) samples in R_a estimation with a minimum error, regarding its low accuracy (88.88%) for each class.

- The Co-occurrence matrix method gives number of input neurons (1024) in the ***ANN*** and gives number of hidden neurons equal to (200), which implies also an average complexity ***ANN*** architecture, but it has the highest number (19/36) samples in R_a estimation with a minimum error, regarding its good accuracy (100%) for each class.
- The bio-orthogonal wavelet method gives quite low number of input neurons (33) at the ***ANN*** and it also gives a low number of hidden neurons (100) which implies a simple ***ANN*** architecture, and it has (14/36) samples in R_a estimation with a minimum error, regarding its good accuracy (100%) for each class.
- The Gabor wavelet method gives lowest number of input neurons (24) in the ***ANN*** and the lowest number of hidden neurons (60) which implies the simplest ***ANN*** architecture, and it has (13/36) samples in R_a estimation with a minimum error, regarding its good accuracy (100%) for each class.

3.2 SECOND DATASET

To prepare the second dataset we collect from Brodatz album the images (D1 to D96) of size 640 × 640. The training and recalling are performed to all images using the same supervised ***ANN*** model with the same parameters values and the same tolerance which is (± 0.005)., Brodatz texture images were used in this work as a second dataset in order to verify the correct accuracy resulted when using the engineering machined surfaces dataset.

3.2.1 RESULTS

The accuracy results of the classified Brodatz textures, as shown in table 2 and figure 9 are between 85.41% and 91.66% and it nearly matches the results obtained by our first data set.

3.3 ANALYSIS AND DISCUSSION

Since we are working as an offline mode image inspection, the number of epochs in the ***ANN*** training phase will not be considered in our comparative study, table 1 shows a comparison between input and hidden layers neurons, while Figure 7 shows the accuracy for the applied five feature extraction methods using the six different multi-class dataset we find that the best accuracy is reached when Co-occurrence, Biorthogonal and Gabor methods are applied while the lowest complexity ***ANN*** Architecture is the Gabor.

In Figure 9 for Brodatz textures we can see nearly a similar accuracy comparison which may mach the one in the first group. With the knowledge of actual surface roughness values (R_a), which measured and stored before and related to ***ANN*** output tolerance, the estimated roughness values are obtained and shown in Figure 8, with minimum error using the various textural analysis methods for the same dataset. While, Tables 3, 4, 5, 6, 7 and 8 show the measured roughness values (multiplied by 10^{-6}) for the **36** machined surfaces with the estimated ones which created by the suggested estimator dimensioned in micron.

A MATLAB7 (the Math Works inc.) based computer code analysis has been developed for image processing and neural network implementation.

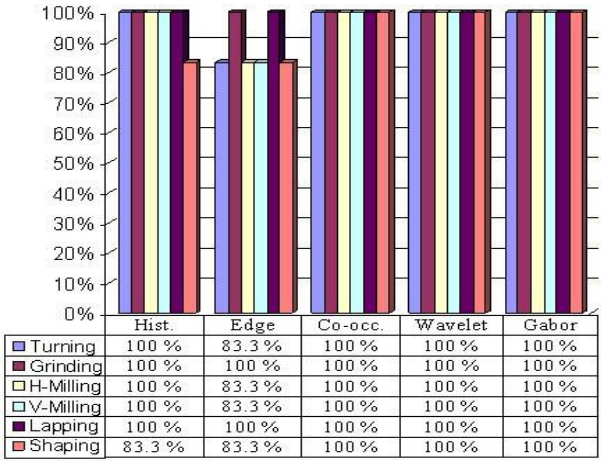

Figure 7: Accuracy of various textural analysis methods using the six different class dataset.

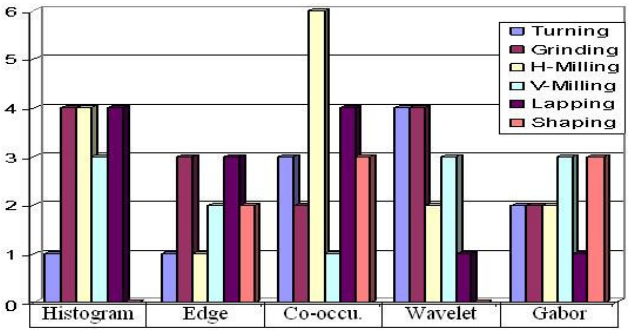

Figure 8: Number of samples estimated with minimum Ra error in each class using the five methods.

Table 1: Number of Neurons in Input and Hidden Layers.

Analysis Method	Histogram	Edge	Co-occ.	Wavelet	Gabor
Input Layer	256	2560	1024	33	24
Hidden Layer	200	200	200	100	60

Table 2: Resulted accuracy of various textural analysis methods using Brodatz textures dataset

Analysis Method	Histogram	Edge	Co-occ.	Wavelet	Gabor
Defined Samples	82	82	88	85	86
Undefined Samples	14	14	8	11	10
Accuracy	85.41	85.41	91.66	88.54	89.58

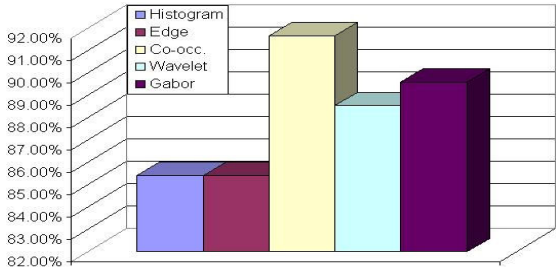

Figure 9: Accuracy comparison for the five texture analysis methods applied to Brodatz textures.

*Table 3: Measured and Estimated **Ra** for **Turning** Samples using the five features extraction methods*

Sample	1	2	3	4	5	6
Measured R_a	***1.900***	***1.200***	***0.800***	***0.896***	***0.701***	***0.200***
Est. R_a Histogram	1.891	1.199	0.797	0.899	0.700	0.199
Est. R_a Edge	**N.D.**	1.199	0.796	0.899	0.700	0.199
Est. R_a Co-Occur	1.891	1.199	0.799	0.899	0.700	0.200
Est. R_a Wavelet	1.901	1.199	0.799	0.897	0.700	0.200
Est. R_a Gabor	1.900	1.200	0.795	0.899	0.699	0.199

*Table 4: Measured and Estimated **Ra** for **Grinding** Samples using the five features extraction methods*

Sample	1	2	3	4	5	6
Measured R_a	***0.109***	***0.500***	***0.200***	***0.100***	***0.060***	***0.030***
Est. R_a Histogram	0.109	0.500	0.199	0.099	0.060	0.029
Est. R_a Edge	0.109	0.500	0.199	0.099	0.059	0.029
Est. R_a Co-Occur	0.110	0.499	0.199	0.099	0.060	0.029
Est. R_a Wavelet	0.110	0.500	0.200	0.100	0.059	0.029
Est. R_a Gabor	0.109	0.500	0.199	0.099	0.059	0.029

*Table 5: Measured and Estimated **Ra** for **H-Milling** Samples using the five features extraction methods*

Sample	1	2	3	4	5	6
Measured R_a	***0.100***	***0.500***	***0.080***	***0.070***	***0.201***	***0.199***
Est. R_a Histogram	0.099	0.499	0.080	0.069	0.200	0.199
Est. R_a Edge	**N.D.**	0.498	0.079	0.069	0.200	0.200
Est. R_a Co-Occur	0.100	0.499	0.080	0.070	0.200	0.199
Est. R_a Wavelet	0.100	0.521	0.080	0.072	0.293	0.207
Est. R_a Gabor	0.100	0.497	0.079	0.070	0.199	0.200

*Table 6: Measured and Estimated **Ra** for **V-Milling** Samples using the five features extraction methods*

Sample	1	2	3	4	5	6
Measured R_a	***1.480***	***1.757***	***0.756***	***0.741***	***0.430***	***0.262***
Est. R_a Histogram	1.489	1.756	0.753	0.741	0.429	0.262
Est. R_a Edge	1.481	1.758	0.755	0.737	0.430	**N.D.**
Est. R_a Co-Occur	1.479	1.754	0.757	0.739	0.429	0.261
Est. R_a Wavelet	1.479	1.756	0.755	0.741	0.429	0.261
Est. R_a Gabor	1.480	1.751	7.550	0.740	0.430	0.261

*Table 7: Measured and Estimated **Ra** for **Lapping** Samples using the five features extraction methods*

Sample	1	2	3	4	5	6
Measured R_a	***0.760***	***0.570***	***0.190***	***0.120***	***0.080***	***0.040***
Est. R_a Histogram	0.759	0.569	0.189	0.120	0.080	0.040
Est. R_a Edge	0.760	0.569	0.189	0.119	0.080	0.039
Est. R_a Co-Occur	0.759	0.569	0.190	0.119	0.080	0.040
Est. R_a Wavelet	0.767	0.572	0.197	0.122	0.086	0.040
Est. R_a Gabor	0.759	0.566	0.190	0.119	0.079	0.039

*Table 8: Measured and Estimated **Ra** for **Shaping** Samples using the five features extraction methods*

Sample	1	2	3	4	5	6
Measured R_a	***2.208***	***2.68***	***2.155***	***2.317***	***1.559***	***8.179***
Est. R_a Histogram	2.204	2.270	2.158	2.319	1.557	**N.D.**
Est. R_a Edge	**N.D.**	2.258	2.154	2.303	1.559	8.170
Est. R_a Co-Occur	2.207	2.260	2.155	2.308	1.559	8.170
Est. R_a Wavelet	2.207	2.260	2.157	2.311	1.557	8.169
Est. R_a Gabor	2.208	2.268	2.151	2.316	1.555	8.156

4. CONCLUSIONS AND FUTURE WORK

We have proposed different approaches based on image processing and multi-layer perceptron supervised neural network that allowed us to classify two different grey level datasets of digitized texture images. The proposed system can establish the relationship between actual surface roughness and texture features of machined surface images (the first dataset), which can be identified and classified based on several textural analysis methods.

The need of using a second textures dataset - which is taken from Brodatz images Album - is to confirm that our algorithm performs efficiently. Moreover, our system can effectively estimate surface roughness value of the first dataset textures with no contact to the specimens and without knowledge about machines parameters (i.e. cutting speed, feed rate, and depth of cut) since we have a measured roughness values reserved as a reference for these textures. The supervised neural network classifier uses ***BPA*** and an adaptive learning rate with momentum term algorithm. Inputs to the ***ANN*** include features vectors related to gray level histogram, edge detection, co-occurrence matrices, Biorthogonal wavelet transformation and Gabor wavelet transformation. This classifier gives accuracy between 88.88% and 100% in classification of the machined work-pieces, while it gives accuracy between 85.41% and 91.66% in classification of the Brodatz textures.

As a future work we plan to use other promising texture classification techniques such as support vector machines. On the other hand we believe that a study that compares the performance of the proposed textural analysis methods with the most recently applied techniques such as ridgelet, curvelet and contorlet transformations would be useful to provide us a more efficient representation for the selected features vector and then leads to more accurate classification for the pattern. Moreover, our algorithm can be implemented on programmable hardware based on the advantage of the simplicity of texture feature extraction criteria.

REFERENCES

[1] Tuceryan and Jain, "Texture Analysis," in The Handbook of *Pattern Recognition and Computer Vision*, World Scientific, 2nd edn., 1998.

[2] Robert m. Haralick, K. Shanmugam, and its hal dinstein, "texture feature for image classification", *IEEE transaction systems*, November 1973.

[3] Wei Min Shi "surface roughness classification using pattern recognition theory," *optical engineering*, vol. 34 No. 6, June 1995.

[4] Sin-Wang-Sonei "On-Line surface defects Detection Using Wavelet-Based Parameter Estimation," *Journal of Manufacturing Science and Engineering*, Volume 125, Issue 1, pp. 21-28 February 2003.

[5] Shmuel Peleg, "Texture Classification Based on the Changing in Image Properties," iris.usc.edu/Information/Iris-Conferences. May, 2002.

[6] Yun Zhang1, Gang Hong1, J. Bryan Mercer2, Dan Edwards2 and Joel Maduck2, "A Wavelet Approach for the Fusion of Radar Amplitude and Optical Multispectral Images," *Multi-Conference on Systemics, Cybernetics and Informatics*, Orlando, July 2005.

[7] Kuang-Chyi, "Accurate Estimation of Surface Roughness from Texture Features of the Surface Image Using an Adaptive Neuro-fuzzy Inference System," *Precision Engineering*, Elsevier, 6 May 2004.

[8] F. luk, and V. H. North, "Measurement of Surface Roughness by a Machine Vision System," *Journal of Physics*, E. Scientific Instruments 22, 977-9800, 1989.

[9] Roberto Marmo, Sabrina Amodio, "Textural identification of carbonate rocks by image processing and neural network," universita adi pavia@ vision. Unipv.it., 2002

[10] S. Arivazhagan, L. Ganesan , S. Padam Priyal, "Texture classification using Gabor wavelets based rotation invariant features," *Pattern Recognition letters,* Elsevier, 2006.

[11] R.E.Reason, O.B.E.,A.R.C.S.D.Sc. (Birm.) "The measurement of surface texture," Macmillan and Co Ltd, 1970.

[12] S.K. Hagra Choudhury, S.K. Bose and A .K. Hagra Choudhury, "Elements of Workshop technology," Media Promotion & Publisher PVT LTD, Bombay, 1991.

[13] Chih-Ming Chen, Chien-Chang Chen and Chaur-Chin Chen "A Comparison of Texture Features Based on SVM and SOM," *IEEE,* 2006.

[14] Taylor Hobson precision "A guide to surface texture parameters," info@taylor_hobson.de

[15] Prithwijit Guha, "Automated visual inspection of steel surface, texture segmentation and development of a perceptual similarity measures," Indian institute of technology, kanpur, April, 2001.

[16] F.J. Seinstra, D. Koelma, "Modeling Performance of low level image processing routines on MIMD Computers ,"Kruislaan 403, 1098 SJ Amsterdam, The Netherlands, fjseins@wins.uva.nl, may 2004.

[17] Ming-Huwi Horng, "Texture features coding method for texture classification," *opt. eng.* 42(1) 228-283, Jan. 2003.

[18] Ming-Huwi Horng, "Texture features coding method for texture classification," *opt. eng.* 42(1) 228-283 Jan. 2003.

.